Journal of Power Sources 271 (2014) 152–159

Contents lists available at ScienceDirect

Journal of Power Sources

journal homepage: www.elsevier.com/locate/jpowsour

Lithium plating in lithium-ion batteries at sub-ambient temperatures investigated by in situ neutron diffraction

Veronika Zinth [a, *], Christian von Lüders [b], Michael Hofmann [a], Johannes Hattendorff [c], Irmgard Buchberger [c], Simon Erhard [b], Joana Rebelo-Kornmeier [a], Andreas Jossen [b], Ralph Gilles [a]

[a] Heinz Maier-Leibnitz Zentrum (MLZ), Technische Universität München, Lichtenbergstr. 1, 85748 Garching, Germany
[b] Lehrstuhl für Elektrische Energiespeichertechnik, Technische Universität München, Arcisstr. 21, 80333 München, Germany
[c] Lehrstuhl für Technische Elektrochemie, Technische Universität München, Lichtenbergstr. 4, 85748 Garching, Germany

HIGHLIGHTS

- Li plating in commercial Li-ion cell at −20 °C studied by in situ neutron diffraction.
- A lower degree of graphite lithiation is found as a result of lithium plating.
- Lithium diffusion into graphite takes place during a 20 h rest period.
- Immediate discharge: no changes in lithiated graphite since Li is oxidized.
- Li plating amounts to 19% of nominal cell capacity.

ARTICLE INFO

Article history:
Received 24 April 2014
Received in revised form
9 July 2014
Accepted 25 July 2014
Available online 4 August 2014

Keywords:
Lithium-ion batteries
Lithium plating
Graphite lithiation
Neutron diffraction

ABSTRACT

Lithium plating in commercial $LiNi_{1/3}Mn_{1/3}Co_{1/3}O_2$/graphite cells at sub-ambient temperatures is studied by neutron diffraction at Stress-Spec, MLZ. Li plating uses part of the active lithium in the cell and competes with the intercalation of lithium into graphite. As a result, the degree of graphite lithiation during and after charge is lower. Comparison of graphite lithiation after a *C*/5 charging cycle fast enough to expect a considerable amount of Li plating with a much slower *C*/30 reference cycle reveals a lower degree of graphite lithiation in the first case; neutron diffraction shows less LiC_6 and more LiC_{12} is present. If the cell is subjected to a 20 h rest period after charge, a gradual transformation of remaining LiC_{12} to LiC_6 can be observed, indicating Li diffusion into the graphite. During the rest period after the *C*/5 charging cycle, the degree of graphite lithiation can be estimated to increase by 17%, indicating at least 17% of the active lithium is plated. Data collected during discharge immediately after *C*/5 charging give further evidence of the presence and amount of metallic lithium: in this case 19% of discharge capacity originates from the oxidation of metallic lithium. Also, lithium oxidation can be directly related to the high voltage plateau observed during discharge in case of lithium plating.

1. Introduction

Today, graphite is used as anode material in most Li-ion batteries [1]. However, because the potential of lithium intercalation into graphite is within 100 mV [2] of the potential of Li/Li^+, the deposition of metallic Li on the graphite anode, so-called Li plating, can occur during fast charging. Whether or not Li plating occurs, depends not only on charging speed, but also on factors like electrode balancing, the electrolyte used in the cell and the temperature during charge [3–8]. For example, several studies by Smart et al. show Li plating can be drastically enhanced at sub-ambient temperatures [2,3,5].

The consequences of Li plating can be severe safety problems, because metallic Li tends to be deposited in the form of dendrites [8–10]. In the worst case scenario, such a dendrite may pierce the separator and short-circuit the cell. On the other hand, Li plating can also lead to loss of active lithium and capacity fading. Plated lithium may react with the electrolyte (adding to SEI growth) or become disconnected from the graphite forming a reservoir of inactive metallic lithium [7,8].

* Corresponding author. Tel.: +49 89 289 11766; fax: +49 89 289 13972.
E-mail address: veronika.zinth@frm2.tum.de (V. Zinth).

http://dx.doi.org/10.1016/j.jpowsour.2014.07.168
0378-7753/

For all these reasons, it is necessary to avoid Li plating, and to be able to avoid Li plating it is necessary to study it more closely and find out exactly when and why it occurs. Unfortunately, studying Li plating ex situ is difficult, since the deposition of metallic lithium is partly reversible. Also, it is difficult and potentially dangerous to open a cell in the charged state because of possible short-circuiting. In the discharged state, on the other hand, only irreversible Li plating can be expected to be present. Studying Li plating in situ is also difficult, because the method has to be sensitive to lithium without being hampered by the cell casing. Apart from a number of electrochemical studies, where a high voltage plateau observed during discharge was used as indication for the presence of lithium plating [2,3,5,11], to our knowledge there is only one other study by Harris et al. where Li plating was observed in situ in an optical half-cell [12].

Neutron diffraction offers a promising alternative to derive information about the processes within a lithium-ion battery. In contrast to x-ray diffraction, it has the advantage of being sensitive to lighter elements (like lithium, oxygen and nitrogen) and the high penetration depth of thermal neutrons makes it possible to investigate Li-ion cells in a non-destructive way. There are two approaches to neutron diffraction on lithium-ion batteries: One is to build special in situ cells, optimized for the diffraction experiment (special geometry, deuterated electrolyte, etc.) [13,14]. The other approach is to use commercial cells, with the benefit that electrochemical performance and balancing of the electrodes are optimized by the manufacturer. A number of studies address the structural changes that take place in anode and cathode materials during charging and discharging of commercial $LiCoO_2$/graphite [15–18] or $LiFePO_4$/graphite [19] cells. Also the influence of cell fatigue on structure and phase composition [17], aging at different temperatures [20] as well as inhomogeneous degradation of large format pouch cells [21] has been studied. While it is usually necessary to charge a lithium-ion battery very slowly (or repeatedly [22]) to collect reasonable neutron diffraction patterns, diffraction data on the strong (002) reflection of graphite and similarly prominent reflections of the intercalation compounds may be collected with a good signal to noise ratio in rather short time intervals of ~5 min, if high neutron flux can be provided. This makes it possible to follow the lithiation and delithiation of graphite in a cell under real-life conditions, as shown in two recent publications on the overcharge of a lithium-ion battery [23] and the current dependency of $Li_{1-x}C_6$ phases within the anode during discharge [24].

In this study Li plating in commercial NMC/graphite cells was studied by neutron diffraction. To enhance Li plating, the measurements were performed at a temperature of −20 °C. The degree of Li intercalation into graphite was monitored during slow (no/little plating expected) and fast (plating expected) charging cycles, subsequent rest periods and discharge. Our observations allow us not only to show the presence of Li plating, but also to estimate its amount and study associated kinetic phenomena.

2. Experimental

For the experiment a commercial 18650-type NMC ($LiNi_{1/3}Mn_{1/3}Co_{1/3}O_2$)/graphite round cell (Molicel IHR18650A by E-ONE MOLI ENERGY CORP.) was used. To our knowledge, the cell electrolyte contains dimethyl carbonate, ethylene carbonate, $LiPF_6$ and propylene carbonate. In a number of cycling experiments prior to the neutron measurements, both room and low temperature behavior were studied. The battery is rated to deliver 1950 mAh nominal capacity. All C-rates in this paper are given relative to this rated capacity.

The cell was cycled using a BioLogic VSP potentiostat. The experimental procedure is shown in Fig. 1: prior to the neutron

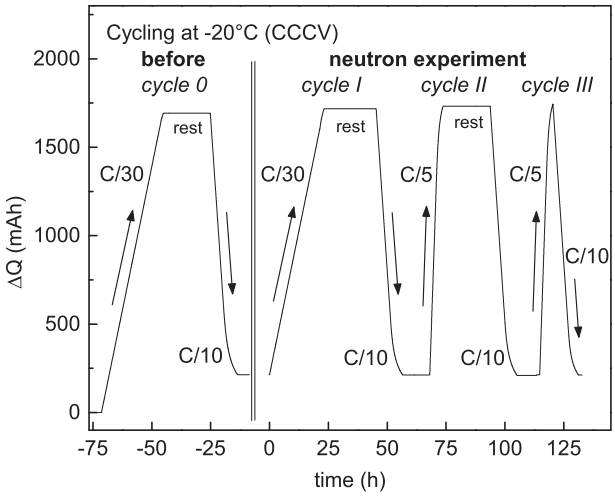

Fig. 1. ΔQ vs. time for cell cycling prior to (cycle 0) and during neutron experiment (cycle I–III) at −20 °C.

experiment, the cell was cycled once (*C*/30) at −20 °C in a freezer and then transferred to a pre-cooled cryostat (cycle 0). When the cell had reached again a temperature of −20 °C, the battery was first charged with a very slow charging rate (*C*/30) to 4.2 V, followed by a constant voltage phase with a cutoff current of *C*/50 (cycle I). Unfortunately, a voltage peak, possibly due to contact problems occurred, the CV phase was triggered too soon and the current rose to a maximum of *C*/15.35 and was above *C*/30 for 39 min. The *C*/30 charge was followed by a rest period of 20 h. After discharge (CCCV, *C*/10, 3.0 V, cutoff: *C*/100), the battery was charged quickly to induce Li plating (cycle II: CCCV, *C*/5, 4.2 V, cutoff: *C*/50), followed by another 20 h rest period and discharge (again CCCV, *C*/10, 3.0 V, cutoff: *C*/100). Additionally, a third charging cycle (CCCV, *C*/5, 4.2 V, cutoff: *C*/50), immediately followed by another *C*/10 discharge without a rest period, was carried out (cycle III).

In situ neutron diffraction data were collected at the instrument Stress-Spec (Heinz Maier-Leibnitz Zentrum [25]). The wavelength was set to $\lambda = 2.1226(1)$ Å; determined using the NIST SRM 640d Si standard powder. The scattering gauge volume was set by a 5×20 mm^2 entrance slit and a 5 mm radial collimator in front of the detector (Fig. 2). Since our preliminary experiments showed that metallic lithium is difficult to detect directly in a battery due to reflection overlap and its comparatively small amount, we focused instead on the strong reflections of the lithium graphite phases, where even small changes in Li content lead to considerably changes. Diffraction data of the strong (002) reflection of graphite and the similarly prominent reflections of the intercalation compounds LiC_{12} and LiC_6 in the scattering angle range of 30–40° 2θ were collected in 5 min intervals throughout the experiment to monitor the changes within the graphite anode of the battery. The integral intensity of reflections was extracted by fitting pseudo Voigt profiles to the data. In case of overlapping reflections, the FWHM (full width at half maximum) was constrained; e.g. one value was refined for all reflections.

3. Results and discussion

3.1. Charging at low temperature

During charge, Li-ions intercalate into the anode of the battery and a stepwise lithiation of the graphite anode via a number of $Li_{1-x}C_6$ phases with lower lithium content, LiC_{12} and finally LiC_6 takes place. Fig. 3 shows diffraction data collected in situ during the

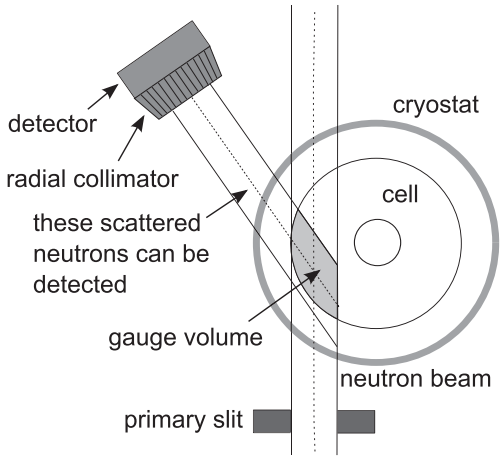

Fig. 2. Schematic setup of the neutron diffraction experiment showing the position of the gauge volume in the cell.

second half of the *C*/30 charging cycle at −20 °C (SOC relative to nominal capacity).

Since Stress-Spec is only a medium resolution powder diffractometer, we do not aim to draw conclusions about details of the intercalation mechanism or the structural details of the $Li_{1-x}C_6$ phases, but to assign the reflections to a phase or Li concentration range and use them to follow the charging progress. Table 1 gives an overview of the observed reflections and their assignment to phases. LiC_6 and LiC_{12} are well characterized and their reflections can be easily identified: at 33.53° 2θ (d = 3.681 Å), the LiC_6 (001) reflection and at 35.04° 2θ (d = 3.526 Å) the LiC_{12} (002) reflection is found (d values in agreement with Refs. [18,19]). Also a shoulder on the LiC_{12} reflection indicates the presence of a third phase with lower Li content and a d-value of 3.462 Å. A recent detailed high resolution neutron powder diffraction study also shows a (002) reflection with d ~ 3.425–3.46 Å and lists a number of phases (IV, V, VIII) present in the same range (compositions from LiC_{72}–$Li_{1-x}C_{18}$) [18]. The first appearance of the reflection at ~3.46 Å upon discharge equals a composition of LiC_{24}. Also Rodriguez et al.

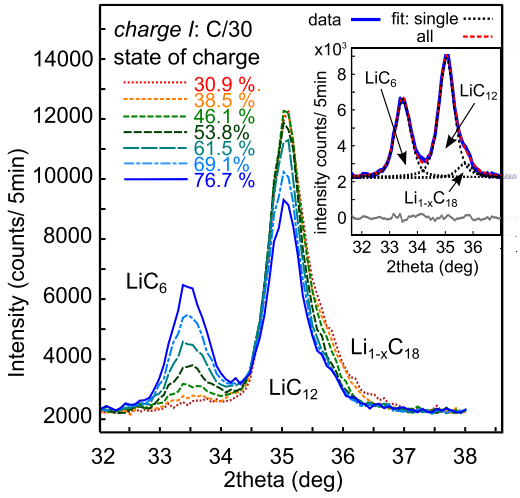

Fig. 3. Diffraction data collected during CCCV *C*/30 charge at −20 °C (CV phase begins after 71.6% SOC); data collected every 135 min are shown, SOC relative to nominal capacity. Inset: Pseudo Voigt profile fitting of data collected at end of charge (blue, solid line), individual contributions of the phases (black, dotted line) and the combined fit (red, dashed line) are shown. (For interpretation of the references to color in this figure legend, the reader is referred to the web version of this article.)

Table 1
Overview over observed reflections and assignment to phases.

Phase	2θ at 2.1226 (Å)	Reflection	d-Values (Å)	Degree of graphite lithiation (%)
LiC_6	33.53	(001)	3.681	100
LiC_{12}	35.04	(002)	3.526	50
"$Li_{1-x}C_{18}$"	35.70		3.462	8.3–34.2[b]
"$Li_{1-x}C_{54}$"[a]	36.66–36.91		3.37–3.4	≤11.2%[b]

[a] Only discharge.
[b] Tentative assignment of Li content in agreement with Senyshyn et al. [18].

tentatively relate a reflection with d = 3.47 Å to LiC_{24} [19]. The same reflection has been assigned to the LiC_{18} phase by Sharma et al. [23]. In the following text we will refer to it as "$Li_{1-x}C_{18}$".

As seen in Fig. 3, at 30.9% SOC, LiC_{12}, $Li_{1-x}C_{18}$ and a small amount of LiC_6 are present. The intensity of $Li_{1-x}C_{18}$ is observed to diminish until approximately 61% SOC, although it never disappears completely in contrast to observations at room temperature. Part of the $Li_{1-x}C_{18}$ seems not to be available for further lithiation at low temperatures, probably because the kinetics are much slower at −20 °C [26]. After 46% SOC has been reached, the LiC_{12} reflection starts to loose in intensity while the LiC_6 reflection intensity rises. However, quite a lot of LiC_{12} remains after the end of charge, and in total only a capacity of 77% (~1503.5 mAh (charge)) relative to the nominal capacity of 1950 mAh is reached. A *C*/100 charge of a battery of the same batch gave a capacity of 1950 mAh at −20 °C (compared to 2050 mAh at room temperature for *C*/100 charge). This shows RT capacity can almost be reached when the charging rate is very small, thus it seems the lower low temperature capacity of ~1500 mAh observed during *C*/20 charge is mainly due to slower kinetics at −20 °C compared to room temperature. Charge transfer resistance [27] or lithium diffusion in graphite [11,28] have been discussed as the rate limiting factor for the charge capability at low temperatures.

3.2. C/5 versus C/30 charge

In situ diffraction data were collected during a second charging cycle at −20 °C with a *C*/5 charging rate to monitor the effects of a "fast" charge at sub-ambient temperatures. Data from this experiment are shown in Fig. 4 (data collected for 5 min every 30 min is shown). Apparently, there are considerable differences from the data of the *C*/30 charge shown in Fig. 3. While for 30–50% SOC the

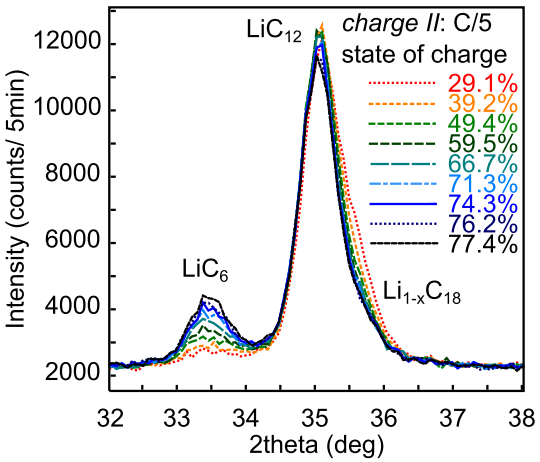

Fig. 4. Diffraction data collected during *C*/5 charge at −20 °C (CV phase begins after 57.3% SOC); data collected every 30 min are shown, SOC relative to nominal RT capacity.

observed reflection intensities and their changes are still similar – intensity of $Li_{1-x}C_{18}$ decreases to a certain level while some LiC_6 is formed – they clearly differ later on. For SOC > 40% only a minor decrease in LiC_{12} reflection intensity is found during the *C*/5 cycle compared to the *C*/30 charge, accompanied by a moderate increase in the LiC_6 reflection intensity. Obviously, much less LiC_{12} is lithiated to form LiC_6 during "fast" *C*/5 charge than during "slow" *C*/30 charge, although the charge capacities for *C*/30 charge and *C*/5 charge are rather similar: 1503.5 mAh (*C*/30) versus 1520.5 mAh (*C*/5). The bigger capacity for the *C*/5 charge can be explained as follows: the (higher) current during *C*/5 charge causes a temperature change in the cell (for example tests in a freezer showed a temperature rise of 1 °C at the cell surface during *C*/5 charge) and supposedly the higher temperature in turn causes a slight increase in cell capacity.

For a better comparison of the diffraction data collected during *C*/30 (cycle I) and *C*/5 charging (cycle II) the LiC_{12}, LiC_6 and $Li_{1-x}C_{18}$ reflections were fitted with a pseudo-Voigt peak profile and the reflection intensities extracted. An exemplary pseudo Voigt profile fitting is shown in the inset in Fig. 4; note the contribution of the $Li_{1-x}C_{18}$ phase to the pattern. The resulting integral intensities are plotted in Fig. 5 relative to the charge ΔQ put into the cell during *C*/30 (cycle I) and *C*/5 charge (cycle II). Due to the faster charging rate, the spacing of data points is bigger for the *C*/5 data. After the onset of the CV phase at 1117 mAh for the *C*/5 charge and at 1396 mAh for the *C*/30 charge the spacing of data points decreases, since the current drops and it takes more time to charge the cell by a certain amount.

A look at Fig. 5 confirms the trends drawn from Figs. 3 and 4: while the behavior of the $Li_{1-x}C_{18}$ reflection intensity is similar for both charging regimes, intensities for LiC_6 and LiC_{12} differ strongly. Both the increase in LiC_6 reflection intensity and the decrease in LiC_{12} reflection intensity lag considerably behind for the *C*/5 charge in cycle II compared to the *C*/30 charge in cycle I.

LiC_6 reflection intensities for the *C*/30 and *C*/5 charge begin to deviate at about $\Delta Q = 950$ mAh (~49% SOC) and differences between reflection intensities of LiC_{12} significantly differ after about $\Delta Q = 1100$ mAh (56.4% SOC). At the end of charge I, the integral intensity for LiC_6 has reached a value of 4000 ± 100 but only 1900 ± 70 (47% of the value after *C*/30 cycle) after charge II at *C*/5. The decrease in LiC_{12} intensity is 29% for *C*/30 charge compared to only 9% for *C*/5 charge. All in all, considerably less LiC_{12} is transformed to LiC_6 during *C*/5 than during *C*/30 charge. Our data clearly show that while the same amount of charge is introduced into the battery for both charging cycles, during *C*/5 charge less lithium moves into the graphite and less LiC_6 (the phase with the highest Li level) is present at the end of charge.

The observed trend in the reflection intensities (and consequently the evolution and formation of $Li_{1-x}C_6$ phases) lends itself to several possible explanations. The charge (and energy) put into the cell in the case of the *C*/5 charge but not stored immediately in the form of lithiated graphite could for example be lost to irreversible side reactions with the electrolyte. However such reactions are expected to be more pronounced at high temperatures than at low temperatures [7]. Another explanation could be that SOC differences are formed because of potential and current density variations in the electrode roll at different distances from the current collector during charge, resulting in local differences in the LiC_6 to LiC_{12} ratio. However, these effects should not increase with decreasing temperatures and are not expected (in the observed magnitude) for the comparatively low *C*/5 charging rate. A third possible explanation is Li plating, which is more pronounced after the charge with the higher current in agreement with literature [4]. In this case part of the charge would be stored in the form of metallic lithium instead of lithiated graphite.

3.3. Relaxation

After the end of both slow (*C*/30) and the fast (*C*/5) charge (cycles I and II), a 20 h rest period was kept to allow for cell relaxation. Diffraction data recorded at the beginning and end of this period are shown in Fig. 6. As expected from the data presented in the last section, at the beginning of the rest period (left), there are big differences in reflection intensity, with less LiC_6 and more LiC_{12} being present after the *C*/5 charge than after the *C*/30 charge. As shown on the right of Fig. 6, after 20 h these differences have almost disappeared, and the LiC_6 as well as the LiC_{12} reflection intensities are very similar in both cases. The time dependent changes of the integral reflection intensities are depicted in Fig. 7. Astonishingly,

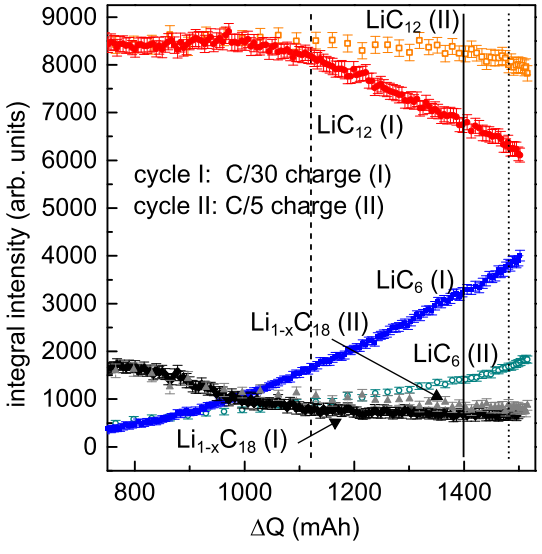

Fig. 5. Integral reflection intensity for LiC_{12} (orange/red), LiC_6 (cyan/blue) and $Li_{1-x}C_{18}$ (grey/black) as a function of capacity for *C*/30 charge (cycle I, onset of CV phase depicted by solid line) and *C*/5 charge (cycle II, onset of CV phase depicted by dashed line, current below *C*/30 by dotted line) relative to the charge ΔQ in mAh put into the cell at −20 °C. (For interpretation of the references to color in this figure legend, the reader is referred to the web version of this article.)

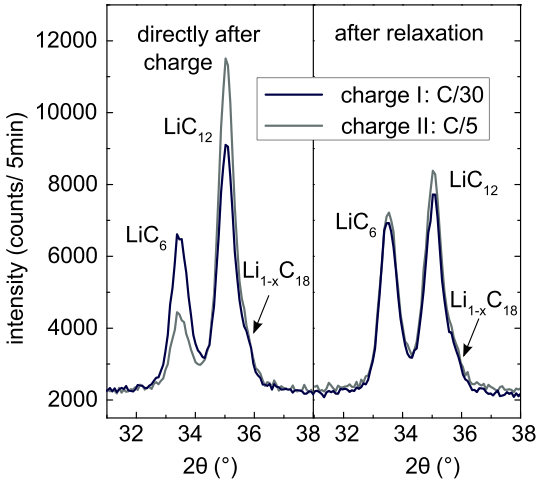

Fig. 6. Comparison of diffraction data directly after *C*/5 (light blue) and *C*/30 (dark blue) charge (left) and after a 20 h relaxation period at −20 °C (right). (For interpretation of the references to color in this figure legend, the reader is referred to the web version of this article.)

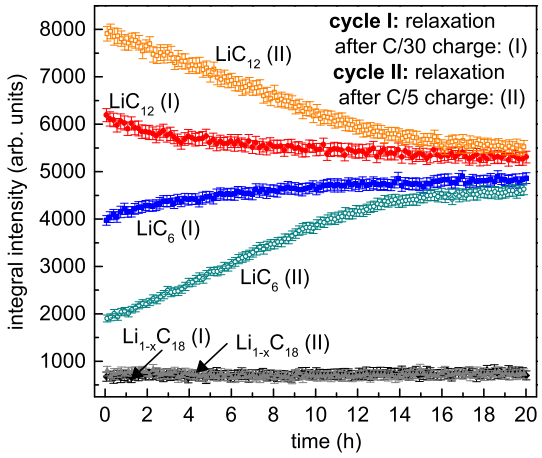

Fig. 7. Changes of integral reflection intensity of LiC_{12} (red, orange) and LiC_6 (blue, cyan) and $Li_{1-x}C_{18}$ (black, gray) during 20 h relaxation at −20 °C after *C*/30 and *C*/5 charge. (For interpretation of the references to color in this figure legend, the reader is referred to the web version of this article.)

there is an increase in the amount of LiC_6 and a decrease in LiC_{12} during relaxation without any additional charge entering the cell. These changes take place both after *C*/5 and *C*/30 charge. However, the effect is much more pronounced after the *C*/5 charge, where the changes are about 3 times larger than the changes after the *C*/30 charge. After *C*/5 charge, the changes in reflection intensity show a linear behavior for the first 600 min (10 h) before slowly leveling out, although small changes in intensity are still found at the end of the 20 h relaxation period. On the other hand, the data points collected after *C*/30 charge show a curving behavior almost from the beginning; changes are smaller here but do not disappear until after approx. 1000 min (16.7 h). For the $Li_{1-x}C_{18}$ reflection intensity, no changes are observed at all during the 20 h of relaxation.

The fact that LiC_{12} is still transformed to LiC_6 even after the end of charge clearly indicates Li intercalation into the anode is still taking place. Due to the sub ambient temperatures, the Li diffusion is slow and the process takes several hours.

These observations rule out irreversible Li loss to side reactions as explanation for the different lithiation degrees after *C*/5 and *C*/30 charge, as in this case no lithium would be available to move into the anode during relaxation. The relaxation behavior could also be explained by spatial inhomogeneities (e.g. more intercalated lithium on one side or a certain area of the electrode) that level out by lithium diffusion. However, in this case lithium diffusion would have to take place over quite a long distance to be responsible for the changes observed, as the scattering gauge volume for the experiment was rather big and covered several electrode layers (~5 × 5 × 20 mm, see also Fig. 2). The long diffusion pathways necessary to enable enough Li-ions to travel into the gauge volume make such an explanation quite unlikely. Using $\tau = x^2/D$ and assuming a solid state lithium diffusion coefficient of $D = 1.9 \times 10^{-11}$ cm^2 s^{-1} as reported by Kulova et al. for the lithium diffusion in graphite at a temperature of −15 °C [26], diffusion by $x = 5$ mm would take approx. 3.7×10^6 h, which is a lot longer than the duration of the experiment.

A more probable explanation for the relaxation behavior shown in Fig. 7 is Li plating. Metallic Li plated on the anode during the charging cycle has a potential equal to zero, while a higher OCV potential is expected for the anode consisting of lithiated graphite (the potential for the LiC_{12} to LiC_6 transition is at 65 mV vs. Li/Li$^+$ [27]). Thus oxidation of the plated Li and (further) reduction of the lithiated graphite takes place, and Li moves from the surface into the anode, transforming LiC_{12} to LiC_6, following the reactions:

$$Li^0 \rightarrow Li^+ + e^-$$

$$Li^+ + e^- + LiC_{12} \rightarrow 2LiC_6$$

Fan et al. [11] report lithium that had been plated in a commercial $LiCoO_2$/graphite cell during charge at −20 °C diffuses into the graphite anode when the cell is warmed to room temperature and kept there for 10 h. The observation that plated Li can intercalate into graphite via a redox reaction agrees with our data. Fan et al. also report that after a 4 h rest at −20 °C the high voltage discharge plateau indicative of Li plating is still observed and conclude no intercalation of the lithium into the graphite has taken place. However, this conclusion seems not to be valid. Our results clearly show there is Li diffusion into the graphite anode even at −20 °C, although with a very slow rate. Assuming a graphite particle size of 5 μm and a diffusion time of 14 h (Fig. 7), a diffusion coefficient of 0.5×10^{-11} cm^2 s^{-1} can be estimated. This value is lower than the values typically reported for lithium diffusion in graphite at room temperature [29] and in same order of magnitude as the diffusion coefficient of 1.9×10^{-11} cm^2 s^{-1} given by Kulova et al. for a temperature of −15 °C.

From the data shown in Fig. 7 the percentage of lithium diffusing into the graphite can be estimated. The structure factor of the (001) LiC_6 reflection is given by $|F(hkl)| = |-6b_C + b_{Li}|$ and that of the (002) LiC_{12} reflection by $|F(hkl)| = |6b_C + b_{Li}|$, where b_C and b_{Li} are the neutron scattering lengths for carbon and lithium, respectively. Reflection intensities can now be corrected by dividing through $|F(hkl)|^2$ to get the relative phase fractions. For these calculations, $Li_{1-x}C_{18}$ was neglected since neither structure nor lithium content is known exactly. This should lead to an overestimation of the degree of graphite lithiation. However, since the $Li_{1-x}C_{18}$ reflection intensity does not change during relaxation, this causes no problem for a relative comparison of the lithiation degree before and after relaxation. This estimation gives 35% LiC_6 and 65% LiC_{12} after the *C*/30 charge in cycle I, which means the average degree of graphite lithiation is 68% (since LiC_6 is 100% and LiC_{12} 50% lithiated). After relaxation, lithiation has increased to 71%. Similarly, after *C*/5 charging in cycle to a lithiation degree of 58% is found that increases to 70% during the 20 h rest period. Thus lithiation of the graphite increases by 4% during rest after *C*/30 charge and by 17% during rest after *C*/5 charge. This means the percentage of lithium plating must have been ≥4% after *C*/30 charge and ≥17% after *C*/5 charge.

3.4. Discharge

As described in the Experimental section, the *C*/5 charge was repeated (cycle III) and then the cell discharged directly (without a rest period) with *C*/10. The data collected during this second *C*/5 charging cycle (cycle III) agree with the first (cycle II). In the following section data measured during the three *C*/10 discharge cycles will be discussed: The first (I) after *C*/30 charge and 20 h rest, the second (II) after *C*/5 charge and 20 h rest and the third (III) directly after *C*/5 charge.

Fig. 8 shows diffraction data collected during discharge (I). As expected, during discharge first LiC_6 is transformed back to LiC_{12} as Li-ions begin to deintercalate. But even before all LiC_6 has been consumed, the shoulder on LiC_{12} indicating the presences of $Li_{1-x}C_{18}$ also begins to grow and broaden. At 31.2% SOC, it is evident that (at least) four phases with different Li content coexist: LiC_6, LiC_{12}, $Li_{1-x}C_{18}$ and a fourth phase with even lower Li content and a reflection at a scattering angle $2\theta = 36.66$–$36.41°$ ($d = 3.37$–3.4 Å). This reflection could belong to a phase denoted (XIV) by Senychyn

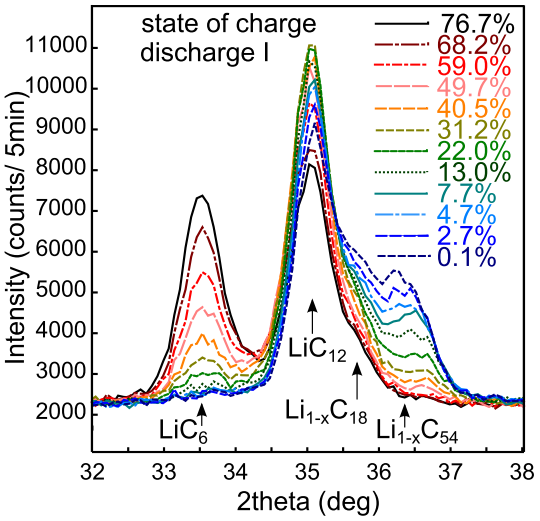

Fig. 8. Diffraction data collected every 55 min during *C*/10 discharge (I) after *C*/30 charge and rest at −20 °C (CV phase begins after 80% depth of discharge (DOD)); SOC relative to rated RT capacity.

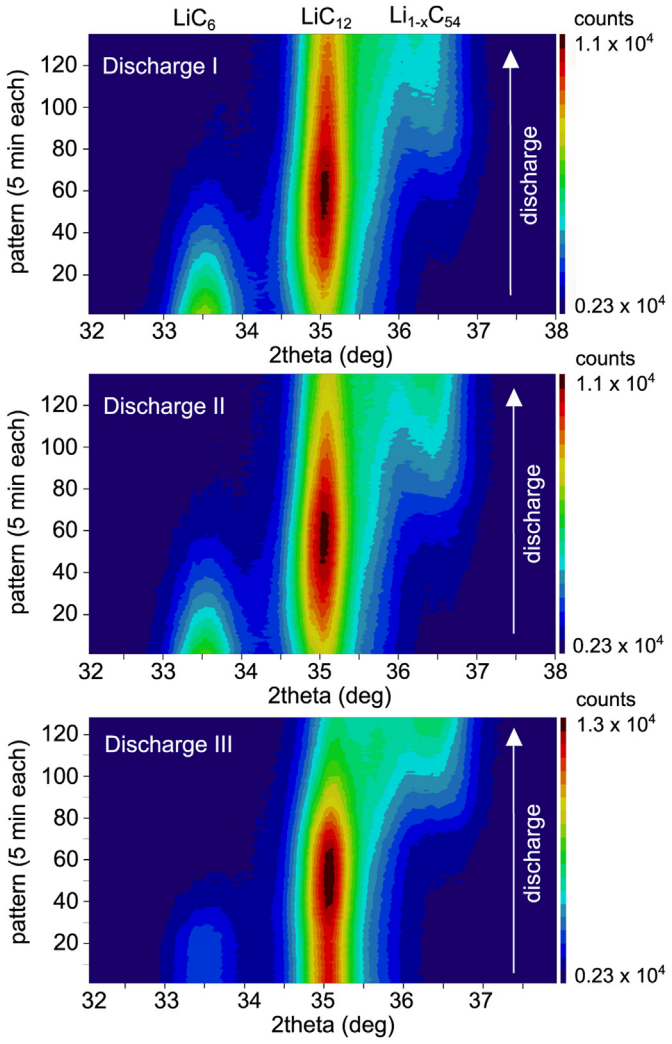

Fig. 9. Diffraction data measured during *C*/10 discharge (I) (top) after *C*/30 charge and 20 h rest, discharge (II) (middle) after *C*/5 charge and 20 h rest and discharge (III) (bottom) directly after *C*/5 charge at −20 °C (red: high intensity, dark blue: low intensity). (For interpretation of the references to color in this figure legend, the reader is referred to the web version of this article.)

et al. [18], with a composition in the range LiC_{54}–LiC_{85}, or a mixture of this phase with the phases XXVIIIp and XXVIIIpp proposed in the same paper. For this study it is sufficient to note a fourth phase "$Li_{1-x}C_{54}$" with a Li content lower than approx. 11.2% is found during discharge. Coexistence of several phases with different Li contents during fast discharge has been found also in other studies [24]. While in situ measurements during slow discharge mostly show the formation of one $Li_{1-x}C_6$ phase after the other with some transitions through two-phase regions [16,18,24], observations during fast discharge are different: Sharma et al. report LiC_{12}, $Li_{1-x}C_{18}$ plus a third lithiated phase (graphite with some remaining lithium) coexist at 63–71% during fast discharge (2 A, 0.8 C) in contrast to slower discharge (0.5 A, 1/5 C) [24]. Slower kinetics at sub-ambient temperatures (especially concerning the Li diffusion within the graphite particles) could lead to the inhomogeneities observed in our experiment during the comparatively slow *C*/10 (195 mA) discharge.

Fig. 9 shows diffraction data collected during discharge I, II and III. Color-coded reflection intensity is displayed against pattern number, with each pattern measured for 5 min during discharge. Since the discharge current (*C*/10) was the same in all cases, patterns collected after the same discharge time should be comparable and only after the onset of the CV phases minor differences can be expected. A comparison of discharge I and II reveals few differences, the reflection intensities during both discharge cycles follow basically the same trends. However, the data collected during discharge III (immediate discharge after *C*/5 charge) obviously differ: there seem to be no changes in reflection intensities of LiC_{12} and LiC_6 during the first ~30 diffraction patterns collected, although the same charge as in discharge I and II must have been extracted from the cell in that time interval.

For a more detailed analysis the integral reflection intensities of LiC_6 and LiC_{12} for the three discharge cycles are compared in Fig. 10. The above observations are confirmed: If the cell is discharged directly after *C*/5 charge, the delithiation of the graphite during discharge does not proceed in the same way it does after a rest period. For discharge cycle III, no change in reflection intensities is observed for the first 110 min. This is in contrast to both discharge I and II, where a considerable decrease in LiC_6 reflection intensity and a corresponding increase in LiC_{12} reflection intensity are found in the same time interval. This means LiC_6 is transformed to LiC_{12} during the early stages of discharge after *C*/5 or *C*/30 charge plus rest (cycles I and II), but if discharge immediately follows *C*/5 charging (cycle III) this is not the case, instead the amount of LiC_6 and LiC_{12} stays constant. The charge taken from the cell during those first 115 min, as well as the Li intercalated into the cathode must therefore originate from a different source than LiC_6.

The presence of metallic lithium seems to be the most probable explanation for the trends seen in Fig. 10: if there is no rest period between charge and discharge, there is no time for the lithium plated on the anode during *C*/5 charge to intercalate into the graphite particles (as observed during the 20 h relaxation period in cycle II). This means metallic Li is still present at the beginning of the discharging process and can be oxidized directly. Since the potential of Li/Li^+ is below that of LiC_6/LiC_{12}, lithium is oxidized first. Lithium oxidation takes place during the first 115 min of the *C*/10 discharge after *C*/5 charge without rest period. The oxidation of the plated Li can be directly linked to a plateau observed in the voltage curve (green curve, upper plot in Fig. 10). The time at which the voltage begins to drop coincidences with the end of the flat range for LiC_6 and LiC_{12} reflection intensities after 115 min during *C*/10 discharge. Smart et al. [5] suggested the width of the plateau to

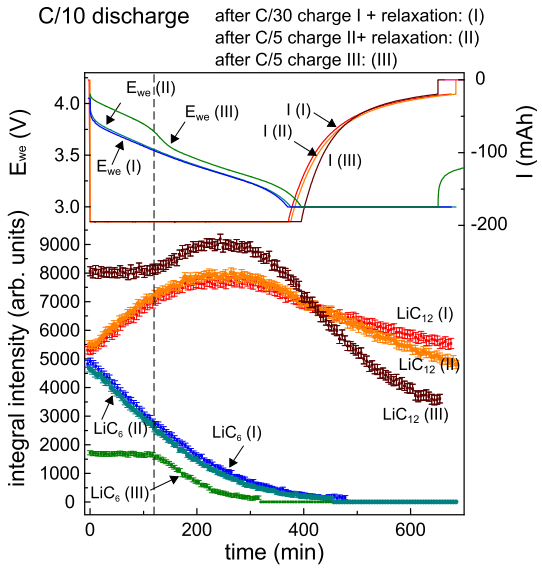

Fig. 10. Integral reflection intensities of LiC_{12} and LiC_6 during $C/10$ discharge after $C/30$ charge (red/blue), $C/5$ charge + rest period (orange/cyan) and $C/5$ charge without rest period (green/pink). Voltage (working potential E_{we}) and current during discharge also shown (top). (For interpretation of the references to color in this figure legend, the reader is referred to the web version of this article.)

be proportional to the amount of metallic Li; the results presented here support this assumption. This implies that a total of 374 mAh (19% of nominal RT capacity) is stored in metallic Li during the $C/5$ charge, e.g. about one fifth of cycle-able Li in the battery is plated. These 19% of metallic lithium found during immediate discharge in cycle III agree well with the 17% of metallic lithium estimated to diffuse into graphite during the 20 h rest period in cycle II, if we account for the uncertainties in the estimation.

Fig. 10 also hints at a possible irreversible part of lithium plating: even after Li oxidation is finished, discharge in cycle III does not proceed in the same way compared to cycle I and II. At the end of discharge a lower intensity is observed for LiC_{12} and higher reflection intensities for the two phases with lower lithium content. This indicates possible irreversible effects (like loss of active lithium) as a result of Li plating followed by immediate discharge. A similar trend, although less pronounced, is found on comparing cycle I and II. Tests on a cell from the same batch pointed to a small capacity loss ($\approx$0.2%) after five successive $C/5$ cycles at −20 °C, each followed by a rest period. The question remains whether Li plating causes more longterm capacity loss if the cell is discharged again directly (as our data seems to indicate) or kept in the charged state long enough to allow for lithium diffusion into the graphite – an interesting issue for future studies on cell aging.

4. Summary and conclusions

To summarize, we studied Li plating in commercial NMC/graphite cells at −20 °C by neutron diffraction. Since Li plating uses a part of the active lithium present in the cell, it competes with the intercalation of lithium into graphite. Neutron diffraction reveals a lower degree of graphite lithiation after a charging cycle fast enough to expect a considerable amount of Li plating ($C/5$ charging rate) in comparison to a slower $C/30$ reference cycle. After charge, ongoing transformation of LiC_{12} to LiC_6 is observed for 17–20 h, indicating Li diffusion into the graphite, with plated metallic lithium as lithium source. In total, the degree of graphite lithiation can be estimated to increase by 4% after $C/30$ charge and by 17% after $C/5$ charge, which gives a lower limit for the amount of lithium plating. During discharge immediately after another $C/5$ charging cycle we find a delay of graphite delithiation (transformation of LiC_6 to LiC_{12}), since plated lithium is discharged first. Thus we can confirm the high voltage plateau observed during discharge is directly linked to the oxidation of metallic lithium and its length is indeed a measure for the amount of Li plating, which in our case amounts to 19% of rated cell capacity.

Although a small amount of irreversibly plated Li is indicated by the small remaining differences between reflection intensities of $C/5$ and $C/30$ charge after relaxation, the observations during relaxation as well as discharge suggest a big part of Li plating is reversible. Metallic lithium in contact with the graphite anode is unstable, reaction with the graphite and lithium diffusion into it takes place. Even at −20 °C, most of the metallic lithium is intercalated after only 13 h. This makes conventional studies on lithium plating difficult: Since the Li diffusion coefficient at 23 °C is reported to be approximately six times the diffusion coefficient at −15 °C [26], at room temperature at most 2 h – possibly less – remain to disassemble a cell or study lithium plating by other methods. This fact further emphasizes the importance of using in situ techniques when Li plating is studied. Our current study shows valuable insights into Li plating in commercial cells can be obtained by neutron diffraction.

Acknowledgments

This work was financially supported by the German Federal Ministry of Education and Research (BMBF) under grant number 03X4633A. We thank Prof. Dr. H. Gasteiger for fruitful discussions, Dr. Weimin Gan for help with the experiment and Dr. Jürgen Peters and Peter Biber for help with the sample environment.

References

[1] B. Scrosati, J. Garche, J. Power Sources 195 (9) (2010) 2419–2430.
[2] R.V. Bugga, M.C. Smart, ECS Trans. 25 (36) (2010) 241–252.
[3] M.C. Smart, B.V. Ratnakumar, L. Whitcanacka, K. Chin, M. Rodriguez, S. Surampudia, in: Battery Conference on Applications and Advances, 2002, The Seventeenth Annual, 2002, pp. 41–46.
[4] S.S. Zhang, K. Xu, T.R. Jow, J. Power Sources 160 (2) (2006) 1349–1354.
[5] M.C. Smart, B.V. Ratnakumar, J. Electrochem. Soc. 158 (4) (2011) A379–A389.
[6] P. Arora, R.E. White, M. Doyle, J. Electrochem. Soc. 145 (10) (1998) 3647–3667.
[7] M. Dubarry, C. Truchot, B.Y. Liaw, K. Gering, S. Sazhin, D. Jamison, C. Michelbacher, J. Electrochem. Soc. 160 (1) (2013) A191–A199.
[8] Z. Li, J. Huang, B. Yann Liaw, V. Metzler, J. Zhang, J. Power Sources 254 (2014) 168–182.
[9] L. Gireaud, S. Grugeon, S. Laruelle, B. Yrieix, J.M. Tarascon, Electrochem. Commun. 8 (10) (2006) 1639–1649.
[10] J. Steiger, D. Kramer, R. Mönig, J. Power Sources 261 (0) (2014) 112–119.
[11] J. Fan, S. Tan, J. Electrochem. Soc. 153 (6) (2006) A1081–A1092.
[12] S.J. Harris, A. Timmons, D.R. Baker, C. Monroe, Chem. Phys. Lett. 485 (4–6) (2010) 265–274.
[13] F. Rosciano, M. Holzapfel, W. Scheifele, P. Novak, J. Appl. Cryst. 41 (2008) 690–694.
[14] M. Roberts, J.J. Biendicho, S. Hull, P. Beran, T. Gustafsson, G. Svensson, K. Edström, J. Power Sources 226 (2013) 249–255.
[15] M.A. Rodriguez, D. Ingersoll, S.C. Vogel, D.J. Williams, Electrochem. Solid State Lett. 7 (1) (2004) A8–A10.
[16] N. Sharma, V.K. Peterson, M.M. Elcombe, M. Avdeev, A.J. Studer, N. Blagojevic, R. Yusoff, N. Kamarulzaman, J. Power Sources 195 (24) (2010) 8258–8266.
[17] A. Senyshyn, M.J. Mühlbauer, K. Nikolowski, T. Pirling, H. Ehrenberg, J. Power Sources 203 (2012) 126–129.
[18] A. Senyshyn, O. Dolotko, M.J. Mühlbauer, K. Nikolowski, H. Fuess, H. Ehrenberg, J. Electrochem. Soc. 160 (5) (2013) A3198–A3205.
[19] M.A. Rodriguez, M.H. Van Benthem, D. Ingersoll, S.C. Vogel, H.M. Reiche, Powder Diffr. 25 (2) (2010) 143–148.
[20] O. Dolotko, A. Senyshyn, M.J. Mühlbauer, K. Nikolowski, F. Scheiba, H. Ehrenberg, J. Electrochem. Soc. 159 (12) (2012) A2082–A2088.
[21] L. Cai, K. An, Z. Feng, C. Liang, S.J. Harris, J. Power Sources 236 (0) (2013) 163–168.
[22] X.-L. Wang, K. An, L. Cai, Z. Feng, S.E. Nagler, C. Daniel, K.J. Rhodes, A.D. Stoica, H.D. Skorpenske, C. Liang, W. Zhang, J. Kim, Y. Qi, S.J. Harris, Sci. Rep. 2 (2012) article number (747).
[23] N. Sharma, V.K. Peterson, J. Power Sources 244 (2013) 695–701.

[24] N. Sharma, V.K. Peterson, Electrochim. Acta 101 (2013) 79–85.
[25] M. Hofmann, R. Schneider, G.A. Seidl, J. Rebelo-Kornmeier, R.C. Wimpory, U. Garbe, H.G. Brokmeier, Phys. B Condens. Matter 385–386 (2006) 1035–1037.
[26] T.L. Kulova, A.M. Skundin, E.A. Nizhnikovskii, A.V. Fesenko, Russ. J. Electrochem. 42 (3) (2006) 259–262.
[27] N. Legrand, B. Knosp, P. Desprez, F. Lapicque, S. Raël, J. Power Sources 245 (0) (2014) 208–216.
[28] S.S. Zhang, K. Xu, T.R. Jow, Electrochim. Acta 48 (3) (2002) 241–246.
[29] M. Park, X. Zhang, M. Chung, G. Less, A. Sastry, J. Power Sources 195 (2010) 7904–7929.